Phase contrast 3D tomography of HeLa cells grown in PLLA polymer electrospun scaffolds using synchrotron X-rays

Bhartiya A[1, 2], Madi K[3], , Disney CM[4], Courtois L[3] Jupe A[5], Zhang F[1,2, 6], Bodey AJ[7], Lee P[8], Rau C[7], Robinson IK[1,2,9], Yusuf M[1,2,10]

1. London Centre for Nanotechnology, University College London, London WC1H 0AH, UK

2. Research Complex at Harwell Rutherford Appleton Laboratory Didcot OX11 0FA, UK

3. 3DMagination Ltd. Atlas Building, Fermi Avenue, Harwell Oxford, Didcot OX11 0QX, United Kingdom

4. School of Mechanical, Aerospace and Civil Engineering, University of Manchester, Manchester, U.K

5. Department of Applied Computing,The University of Buckingham

6. Department of Electrical and Electronic Engineering, Southern University of Science and Technology, Shenzhen 518055, People's Republic of China

7. Diamond Light Source, Oxfordshire, OX11 0DE, UK

8. Mechanical Engineering, University College London, WC1E 7JE, UK.

9. Condensed Matter Physics and Materials Department, Brookhaven National Laboratory, Upton, New York 11973, USA.

10. Centre for Regenerative Medicine and Stem Cell Research, Aga Khan University, Karachi, Pakistan

Corresponding author

Dr Mohammed Yusuf

ucanymo@ucl.ac.uk; Mohammed.yusuf@aku.edu

Keywords: 3D culture, electropun polymer scaffold, Xray CT, Synchrotron, Image analysis, Avizo

Abstract

Advanced imaging is useful for understanding the 3D growth of cells. X-ray tomography serves as a powerful noninvasive, nondestructive technique that can fulfill these purposes by providing information of cell growth within 3D platforms. There are a limited number of studies taking advantage of synchrotron X-rays that provides a large field of view and suitable resolution to image cells within specific biomaterials. In this study X-ray synchrotron radiation microtomography at Diamond Light Source and advanced image processing were used to investigate cellular infiltration of HeLa cells within poly-L-lactide (PLLA) scaffolds. This study demonstrates that synchrotron X-rays using phase contrast is a useful method to understand 3D growth of cells in PLLA electrospun scaffolds giving a large field of view. Two different fiber diameter (2 and 4 μm) scaffolds with different pore sizes, grown over 2, 5 and 8 days in vitro were examined for infiltration and cell connectivity. After performing visualization by segmentation of the cells from the fibers, the results clearly show deeper cell growth and higher cellular interconnectivity in the 4 μm fiber diameter scaffold.

This indicates the potential for using such 3D technology to study cell/scaffold interactions to understand disease and for future medical use.

Introduction

Tissue engineering is an expanding interdisciplinary field combining life, material and bioengineering sciences, aiming to restore damaged tissue and organs [1, 2]. The goal is to produce a three-dimensional (3D) construct(s) that uses live cells supported by a scaffold that replicates in vivo conditions for successful tissue/organ replacement. These 3D scaffolds provide support and allow cellular growth processes, such as cell adhesion, migration, proliferation and differentiation to take place [3, 4], maintaining tissue homeostasis *in vitro* [5]. Scaffoldsserve as suitable in vitro models gor cell growth in which *in vitro* cancer cell behavior can be investigated [6, 7, 8].. Before designing any experiment the type and design of scaffold , growth factors, the extracellular matrix (ECM) and cells of choice [9] need to be selected carefully for the required application.

A number of different biomaterials have been developed for tissue engineering applications. This includes naturally both derived and synthetic polymers. [10]. Using electrospinning technology, highly porous scaffolds with interconnected pores or random fiber networks can be produced [11-12]. Materials for scaffolds includes poly(L-lactic acid) (PLLA) that have received approval from US Food and Drug Administration (FDA) for human clinical use [13, 14], making it a material of interest. Furthermore it can be easily processed, can degrade to natural metabolites, and has mechanical properties that can be adjusted to specific requirements needs [15]. Scaffold fiber diameter can range from nano- to microscale [16, 17, 18] and should ideally resemble the extracellular matrix dimensions.

To understand scaffold characteristics such as architecture, cell infiltration and growth of cells, imaging serves as a useful tool [19]. As scaffolds can have varied structure in the depth dimension, certain characteristics are not observable using standard 2D imaging methods. For example, scanning electron microscopy (SEM) has been routinely used to image the surface of scaffolds seeded with cells [20, 21].

The microscopy technique selected is usually dependent on the thickness of the scaffold and it is clear that new imaging approaches for tissue engineering applications need to be further explored and developed [22]. Imaging of cells grown in scaffolds using standard light microscopy poses several problems as the 3D structure cannot be fully characterized mainly due to the thickness of the scaffold and the light diffracting [23]. Fluorescent labeled adherent live cells can be imaged using confocal microscopy can scan samples with a greater depth of up to 350 μm but this depends on the property of the sample [24, 25]. Higher resolution can be obtained using multiphoton fluorescence microscopy that allows simultaneous excitation at multiple long wavelengths results in fluorescence [26]. These techniques are useful but require fluorescent labelling of the sample and give sparse information. Furthermore, high light intensities often lead to fluorophore bleaching and phototoxic effects [27]. Both fluorescence and confocal microscopy cannot see the interior of the ‘opaque’ scaffold. To understand complete cell behavior within the scaffold, 3D rendering of sections imaged using confocal after cryofixing fluorescent cells has been done [28]. Furthermore, obtaining 2D sections and performing 3D reconstructions either by confocal [29] or focused ion beam (FIB-SEM) [30] is a disruptive, tedious and can be destructive due to the need for sectioning or staining.

Nondestructive 3D imaging at high resolution can be achieved using X-ray tomography [31] of large samples that are up to a few cm^3, with high resolutions of sub-μm and allows quantitative measurements [32]. Microcomputed tomography (microCT) has been used widely for biological sample imaging that allows deep penetration into the sample [32, 33]. The method uses 2D X-ray images at different angles around the sample (usually 180° or 360°). After 3D reconstruction, sophisticated analysis can be done using different software tools [34]. This technology has been used for imaging scaffolds containing cells using lab based X-ray systems by phase contrast [11, 35, 36]. Even though the X-rays can penetrate through the sample and provide high resolution (150 nm) the main disadvantage is the limited field of view [16]. Better phase contrast can be achieved using microCT systems generated in a synchrotron to image cells, as synchrotron source generates high spatial coherence and high flux [37]. In addition the use of heavy metal staining can be eliminated when performing in phase contrast imaging which is advantageous to keep structural details intact [46].

In this study non-toxic and FDA approved electrospun PLLA scaffolds were used. Our study focused on evaluation and comparison of 2 different fiber diameter scaffolds. An immortal HeLa cancer cell line was selected as it is the most widely used model cell line that has contributed towards many medical science discoveries. They grow fast with a doubling time of 24 hours, making them ideal for developing protocols [45].This paper demonstrates the use of synchrotron X-ray microCT for imaging cells grown in electrospun PLLA scaffolds giving a large field of view. Also, the effect of different scaffold fiber/pore sizes on cancer cell growth and infiltration was tested. Unstained cells were seeded and measured at three different time points in two different fiber/pore sized scaffolds.

Material and Method

Sample Preparation

‘’The scaffold material was purchased from the Electrospinning Company, UK. https://www.electrospinning.co.uk/. The selected electrospun scaffolds were made of PLLA and have 2 μm and 4 μm diameter fibers with random orientations. The pore sizes are 14.8 ± 4.3 μm and 22.7 ± 8.1 μm for the 2 μm and 4 μm diameter fiber scaffolds, respectively. The scaffolds were in the form of 2 cm diameter disks with a thickness of around 50 μm. HeLa cells were obtained from Prof Stanley Botchway (Central Laser Facility, Science and Technology Facilities

council, UK). These cells were grown in the scaffold material following previously published protocols [16, 21]. Briefly, HeLa cells were grown in electrospun porous poly(L-lactide);(PLLA) scaffolds for 2, 5 and 8 days. The scaffolds containing cells were then fixed using 2.5% (vol/vol) glutaraldehyde (Sigma Aldrich, UK) in 0.1 M cacodylate buffer Sigma Aldrich, UK); (pH 7.2) for 2 h. Fixing the samples was done to preserve samples at room temperature. Cell samples were not stained with any heavy metals. After the samples were washed three times with 0.1 M cacodylate buffer (pH 7.2), followed by a dehydration using a series of ethanol solutions (70%, 85%, and 100%). The samples were finally dried at room temperature using hexamethyldisilazane (Sigma-Aldrich, UK) for 5 min. for Before X-ray scanning, scaffolds were prepared into thin strips by cutting the scaffold material using a sharp blade or scissors. Once the strips were made the scaffold material was carefully placed within 1.8 mm diameter kapton tubing (Goodfellow, UK) ensuring there was no folds. Mounting of the sample in the kapton tubing for the microCT was done as described previously [16] by gluing the kapton tubing onto a pin holder that then attached onto the rotation stage.''

.

Beamline I13-2 at Diamond Light source for X-Ray tomography

The in-line phase contrast microtomography on I13-2 beamline was used at high resolution (circa 1 μm), using pink beam (5-35 keV) to obtain phase contrast on the samples [38, 39, 40]. Tomography scans with the pco.edge 5.5 detector at 8x total magnification was performed. The field of view was 2.1mm x 1.8mm with an effective pixel size of 0.81 μm. The high flux of the X-ray beam allowed tomography datasets to be recorded rapidly. The exposure time was set to 20 ms per radiograph with a 0.045 degree step size, obtaining 4001 projections per data set. A filtered back projection algorithm with dark- and flat- field correction reconstructed 3D volumes from the projections using Diamond Light Source (DLS) software DAWN (41).

Data Analysis: Data was analysed using powerful dedicated graphic workstations at I13-2 (DLS) [38, 41]. After reconstruction, the 3D dataset were converted from 32-bit tiff images into 8-bit images using Image J/Fiji software. The kapton tubing artifacts that were seen around the scaffold material were cropped out reduceding the size of the data. A region of interest was created from the full data set and had dimensions of 722 x 522 x 667 voxels. A 2D slice or plane in XZ was aligned with the surface and used to determine visually the apparent growth of cells within the scaffold as a first inspection, This was done for all the 2 μM fiber and 4 μM fiber **diameter scaffold** samples and the different days (2, 5 and 8 days).

Image processing

The image processing was performed using Thermo Scientific Amira-Avizo 9.5 software. The 3D dataset were filtered using a non-local means algorithm to de-noise the images while preserving the boundaries between the scaffold fibers and the cells. The scaffold and the cells were separately segmented using a 3D region growing algorithm. A euclidean distance map was computed from a binary mask that includes both scaffold fibers and pores. A python script was then developed to quantify the volume of cells as a function of the distance from the two opposite scaffold edges. At a given depth, the volume fraction of cells defined as the volume of cells divided by the volume of both, fibers and pores, was also calculated. The script was adjusted to quantify the volume of cells from the upper scaffold surface where the cells have grown.

Results and Discussion

The X-ray scans gave a large field of view (2.1 mm x 1.8 mm) with cells clearly visible on the surface of the scaffold after aligning the tomograms (Figure 1A).

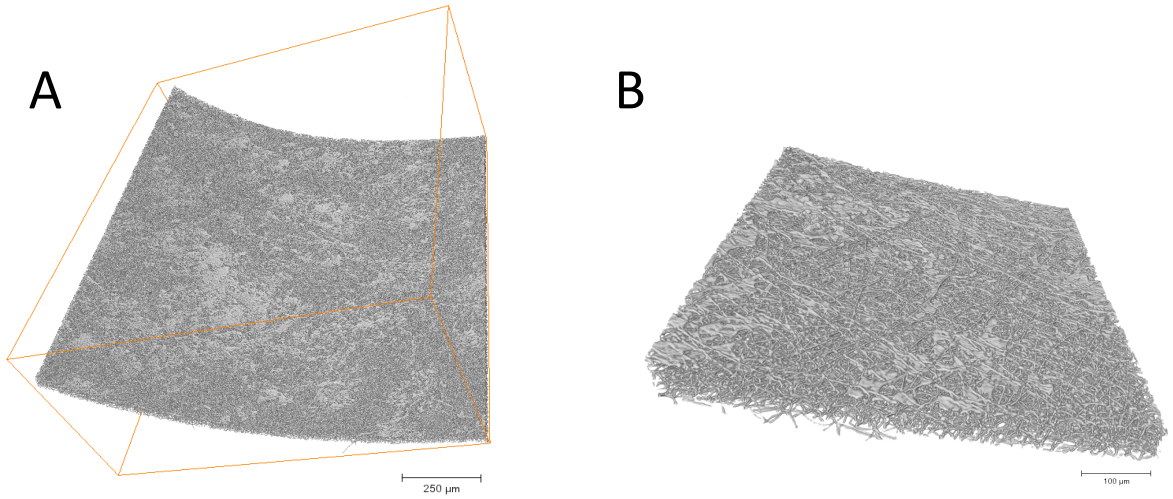

Figure 1. 3D X-ray image of cells grown in electrospun scaffolds. A) A full field of view 2.1 mm x 1.8 mm showing a 3D PLLA scaffold image with cells (white) distributed on the surface of the scaffold. Scale bar 250 µm. B) Subvolume of A showing an enlarged section with cellular detail on the surface of the scaffold visible including individual scaffold fibers. Scale bar 100 µm.

Obtaining a large field of view is important as cells can grow in different orientations according to the scaffold architecture. The subvolumes show clear distribution of cells on the seeded surface with reduced contrast difference between the scaffold and cells observed for all the samples used in the study. Figure 1B and Supplementary 1A-F shows tomograms of 2 µm and 4 µm fiber diameter scaffolds with cells grown for different durations (2, 5 and 8 days). It is also important to examine growth inside the scaffolds. To visualize cell distribution within the two scaffold types (2 µm and 4 µm fiber diameter) over the different days (2, 5 and 8 days), the volume fraction of cells as a function of the distance from the scaffold surface was measured. The 4 µm fiber diameter scaffold, 2 days was not included as there was very few cells to segment so was excluded from the analysis (Supplementary Figure 1D). Each voxel (0.81µm) was measured from the surface where the cells migrated deeper into the scaffold over time after cell seeding. Figure 2A shows cells in the 2 µm fiber diameter scaffold migrate to a depth of approximately 10 µm after 2 days to 16 µm after 5 days and 15.2 µm after 8 days. In comparison cells in the 4 µm fiber diameter scaffold showed a depth of 43.2 µm and 48.8 µm after 8 days (Figure 2B). Connected cells in the entire scaffold have been displayed in 3D using different colors to identify clusters (Fig 2C, 2D and Supplementary Figure 2A-C). The 4 µm fiber diameter scaffold at 8 days has 1 color (in blue) because all the cells are interconnected (Fig 2D) whereas the other cells are clustered in multiple colors (Fig 2C, Supplementary Fig 2A-C). These clusters show that the cell density is increasing with growth of cells from 2 days to 8 days. Supplementary Figure 3 shows cells on the surface of the 2 µm fiber diameter scaffold.

D

B

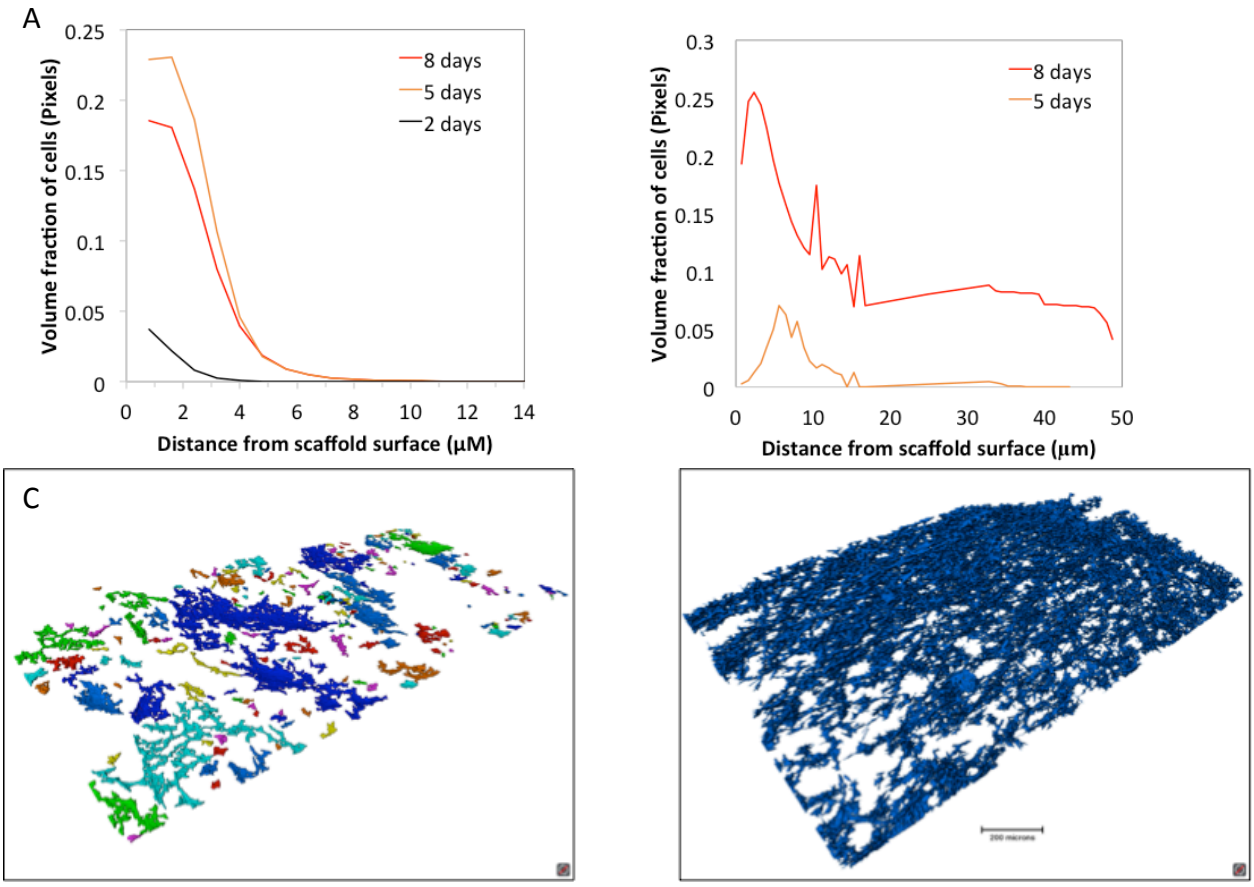

Figure 2. Volume fraction of cell voxels as a function of the distance from the scaffold surface. a) graph showing comparison between cells grown for 2, 5 and 8 days for the 2 µm fiber diameter scaffold b) graph comparison between cells grown for 5 and 8 days for the 4 µm fiber diameter scaffold.
3D visualization of the whole cells with each color a group of cells that are connected. C) 8 days for the 2 µm fiber thick scaffold b) 8 days for the 4 µm fiber thick scaffold. Scale bar 200 µm.

The reconstructed images of cells cultured on fibrous scaffolds showed that they can grow within both type of fibrous scaffolds used. Cells attached to the surface of the 2 µm fiber diameter scaffold and distributed mainly on the surface whereas the cells distributed on both the surface and within (z) the 4 µM fiber diameter scaffold (Figure 3).

A B

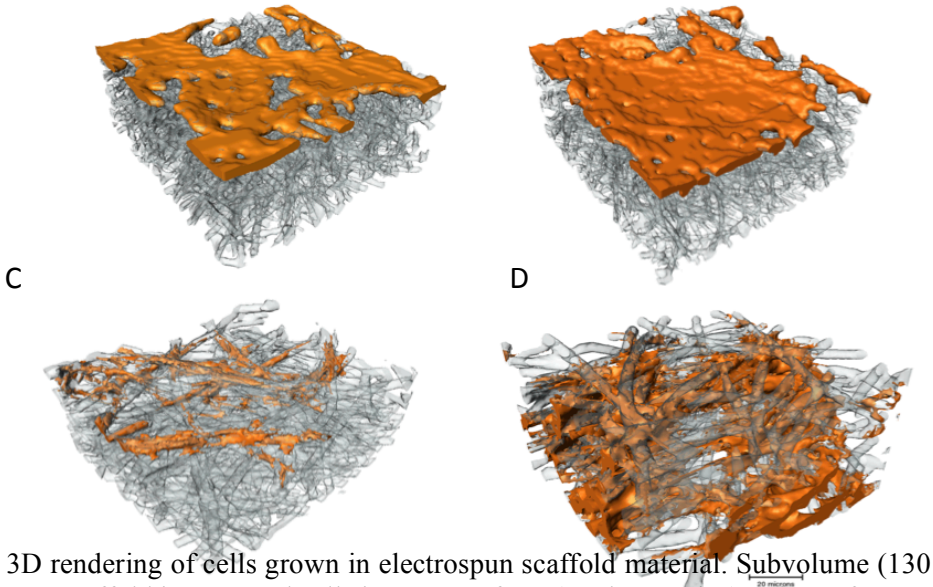

Figure 3. 3D rendering of cells grown in electrospun scaffold material. Subvolume (130 µm) of 2 µM fiber diameter scaffold in grey and cells in orange after A) 5 days and B) 8 days of growth. Subvolume (130 µM) of 4 µm fiber diameter scaffold in grey and cells in orange after C) 5 days and D) 8 days of growth. Scale bars for B and C are 20 µm.

The 2 µm fiber diameter scaffold was not suitable for cells to infiltrate into the pore between and among fibers. However if cells were left in the 2 µm diameter scaffold for longer then maybe the cells would have migrated further inside the scaffold material. The 4 µm diameter scaffold has a larger pore size (15-30 µm) than the 2 µm (5-10) fiber scaffold. It is already known that the 3D matrix physical properties such as pore size and porosity and fiber diameter can affect cell morphology, attachment and function [47, 48]. The scaffold acts as a structural support and needs pores to allow cell attachment proliferation and migration. The cells should have access to oxygen and nutrients to cells and will enable waste products removal. The scaffold should be biocompatibale and appropriate mechanical properties [13].

The use of X-ray tomography together with sophisticated 3D analysis has been demonstrated well in this study as well as recent studies investigating different polycaprolactone scaffolds for bone tissue regeneration [49, 50] and after checking the effect of mineralisation behaviour of $CaCO_3$ deposited on such scaffolds followed by 2 plasma treatment [51]. It is evident that the future will involve using such methods not only for investigating scaffold characteristics but will combine detailed cell analysis investigating cell adhesion, growth, viability morphology and differentiation [51]. Nevertheless, X-ray microCT methodology is costly and involves having access to a synchrotron facility but has advantages requiring no staining, high flux. As the large field of view comes at the cost of spatial resolution, precise analysis of nanofibers cannot be achieved

(49). We are also now witnessing 3D imaging studies moving towards cryo imaging of cells to understand understanding scaffolds-cell interactions. Cryo FIB-SEM has been used to evaluate cryo prepared electrospun nanofibre scaffolds on which osteoblasts were grown [52]. Even though cryo imaging using soft x-ray cryo microscopy of unstained cryofixed cells in the water window range have been imaged it cannot be used to image scaffold-cells due to the thickness of the samples [53].

Conclusion

Overall this study demonstrated that X-ray microtomography with inline phase contrast serves as a suitable imaging method for the 3D observation of cell grown in electrospun scaffolds as it allows high penetration through the sample, is nondestructive and does not require any staining. The 3D scaffolds provide support to the cells and the cells show clear contact with one another. Clear segmentations can be done in which cells can be separated from the scaffold, allowing us to understand the growth of cells within different scaffold types. Comparisons of the two scaffolds showed that HeLa cells in the 2 μm fiber diameter scaffold, with smaller pore sizes, did not penetrate into the material and formed cell sheets on the scaffold surface. Conversely, cells grown in the 4 μm scaffold fiber penetrated inside and grew within the scaffold. The results also show that cells are more interconnected in the 4 μm fiber diameters caffold after 8 days of growth penetrating throughout the entire 50 μm scaffold. This study will allow us to identify suitable platforms for cancer cell biology and metastasis, in which we will be able to understand the complicated behavior of cells. Imaging the interior of scaffolds will also serve useful for other applications such as tissue regeneration and stem cell generation [51].

Acknowledgements

The authors would like to acknowledge the Biotechnology and Biological Sciences Research Council (BBSRC, UK) through grant BB/H022597/1. I.R was partly supported by Brookhaven National Laboratory was supported by the U.S. Department of Energy, Office of Science, Office of Basic Energy Sciences, under Contract No. DE-SC0012704. C.M.D. was supported by an EPSRC & MRC Centre for Doctoral Training (CDT) Regenerative Medicine (EP/L014904/1) studentship and EPSRC Doctoral Prize Fellowship (EP/R513131/1). F. Z. acknowledges funding

from the National Natural Science Foundation of China (No. 11775105). The authors would like to thank the Electrospinning Company, Rutherford Appleton Laboratory, Harwell, Oxford, UK for regular discussion on scaffold material. The authors would also like to acknowledge the ongoing support of Professor El-Nasir MA Lalani of the Centre for Regenerative Medicine and Stem Cell Research at the Aga Khan University, Karachi.

References

1. Langer R, Vacanti JP. Tissue Engineering. Science. 1993;260(5110):920–7.

2. Gurtner GC, Callaghan MJ, Longaker MT. Scaffolds and cells for tissue regeneration: different scaffold pore sizes—different cell effects. Progress and Potential for Regenerative Medicine. Annu Rev Med. 2006;58:299–312.

3. Bruzauskaite I, Bironaite D, Bagdonas E and Bernotiene E. Cytotechnology. 2016; 68(3): 355–369.

4. Fletcher DA, Mullins RD. NIH Public Access. 2010;463(7280):485–92.

5. Lenas P, Moos M, Luyten FP. Developmental Engineering: A New Paradigm for the Design and Manufacturing of Cell-Based Products. Part I: From Three-Dimensional Cell Growth to Biomimetics of In Vivo Development . Tissue Eng Part B Rev. 2009;15(4):381–94.

6. Rijal G, Bathula C, Li W. Application of Synthetic Polymeric Scaffolds in Breast Cancer 3D Tissue Cultures and Animal Tumor Models. Int J Biomater. Hindawi; 2017;2017:1–9.

7. Rijal G, Li W. A versatile 3D tissue matrix scaffold system for tumor modeling and drug screening. Sci Adv. 2017;3(9):1–16.

8. Fischbach C, Chen R, Matsumoto T, Schmelzle T, Brugge JS, Polverini PJ, et al. Engineering tumors with 3D scaffolds. Nat Methods. 2007;4:855–60.

9. Zhang S. Designer self-assembling Peptide nanofiber scaffolds for study of 3-d cell biology and beyond. Adv Cancer Res. 2008;99:335–62.

10. Bhattarai DP, Aguilar LE, Park CH and Kim CS. A Review on Properties of Natural and Synthetic Based Electrospun Fibrous Materials for Bone Tissue Engineering. 2018; 14;8(3):E62

11. Pan Z, Ding J. Poly(lactide-co-glycolide) porous scaffolds for tissue engineering and regenerative medicine. Interface Focus. 2012;2(3):366–77

12. Lannutti J, Reneker D, Ma T, Tomasko D, Farson D. Electrospinning for tissue engineering scaffolds. Mater Sci Eng C. 2007;27(3):504–9.

13. Ma PX. Scaffolds for tissue fabrication. 2004; Mater. Today 7(5): 30–40.

7.
14.Thomson RC, Wake MC, Yaszemski MJ, et al. Biodegradable polymer scaffolds to regenerate organs. Adv. Polym. Sci. 1995; 122:245–274.

15. Lin Y, Wang L, Zhang P, Wang X, Chen X, Jing X, Su Z. Surface modification of poly(L-lactic acid) to improve its cytocompatibility via assembly of polyelectrolytes and gelatin. Acta Biomater. 2006, 2, 155–164.

16. Bradley RS, Robinson IK, Yusuf M. 3D X-Ray Nanotomography of Cells Grown on Electrospun Scaffolds. Macromol Biosci. 2017;17(2):1–8.

17. Subbiah T, Bhat GS, Tock RW, Parameswaran S, Ramkumar SS. Electrospinning of nanofibers. J Appl Polym Sci. 2005;96(2):557–69.

18. Li W-J, Laurencin CT, Caterson EJ, Tuan RS, Ko FK. Electrospun nanofibrous structure: A novel scaffold for tissue engineering. J Biomed Mater Res. 2002;60(4):613–21.

19. Sengers BG, Taylor M, Please CP, Oreffo ROC. Computational modelling of cell spreading and tissue regeneration in porous scaffolds. Biomaterials. 2007;28(10):1926–40.

20. Millas ALG, McKean R, Stevens R, Yusuf M, Silveira JVW, Puzzi MB, et al. Fabrication of Electrospun Scaffolds Incorporating an Amazonian Therapeutic Oil from the Copaifera Species for Wound Care Applications. J Biomater Tissue Eng. 2014;4(3):217–20.

21. Yusuf M, Millas ALG, Estandarte AKC, Bhella GK, McKean R, Bittencourt E, et al. Platinum blue staining of cells grown in electrospun scaffolds. Biotechniques. 2014;57(3).

22. Appel AA, Anastasio MA, Larson JC, Brey EM. Imaging challenges in biomaterials and tissue engineering. Biomaterials. 2014;71(11):3831–40.

23. Graf BW, Boppart SA. Imaging and Analysis of Three-Dimensional cell culture Models. Methods Mol Biol. 2010;591(3):185–99.

24. Cox G, Sheppard CJR. Practical Limits of Resolution in Confocal and Non-Linear Microscopy. Microsc Res Tech. 2004;63(1):18–22.

25. Boustany NN, Boppart SA, Backman V. Microscopic Imaging and Spectroscopy with Scattered Light. Annu Rev Biomed Eng. 2010;12(1):285–314.

26. Georgakoudi I, Rice WL, Hronik-Tupaj M, Kaplan DL. Optical Spectroscopy and Imaging for the Noninvasive Evaluation of Engineered Tissues. Tissue Eng Part B Rev. 2008;14(4):321–40.

27. Pampaloni F, Reynaud EG, Stelzer EHK. The third dimension bridges the gap between cell culture and live tissue Francesco. Nat Rev Mol Cell Biol. 2007;8(10):839–45.

28. Roy D, Steyer GJ, Gargesha M, Stone ME, Wilson DL. 3D Cryo-Imaging: A Very High-Resolution View of the Whole Mouse. Anat Rec (Hoboken). 2009. 292(3): 342–351.

29. Dey J, Nair A, Thevenot P, Yang J, Tang L. Method to Analyze Three-Dimensional Cell Distribution and Infiltration in Degradable Scaffolds. Tissue Eng Part C Methods. 2008;14(4):319–31.

30. Stachewicz U, Qiao T, Rawlinson SCF, Almeida FV, Li WQ, Cattell M, et al. 3D imaging of cell interactions with electrospun PLGA nanofiber membranes for bone regeneration. Acta Biomater. 2015;27:88–100.

31. Bradley RS, Withers PJ. Correlative multiscale tomography of biological materials. MRS Bull. 2016;41(07):549–56.

32. Plessis A du, Broeckhoven C, Guelpa A, Gerhard Le Roux S. Laboratory x-ray micro-computed tomography: A user guideline for biological samples. Gigascience. 2017;6(6):1–11.

33. Mizutani R, Suzuki Y. X-ray microtomography in biology. Micron. 2012;43(2–3):104–15.

34. Kalender WA. X-ray computed tomography. Phys Med Biol. 2006;51(13):R29–43.

35. Shepherd D V, Shepherd JH, Best SM, Cameron RE. 3D imaging of cells in scaffolds: direct labelling for micro CT. J Mater Sci Mater Med. 2018;29(6):1–4.

36. Dorsey SM, Lin-Gibson S, Simon CG. X-ray microcomputed tomography for the measurement of cell adhesionand proliferation in polymer scaffolds. Biomaterials. 2009;30(16):2967–74.

37. Zehbe R, Schmitt VH, Kirkpatrick CJ, Brochhausen C. High resolution X-ray tomography – three-dimensional characterisation of cell–scaffold constructs for cartilage tissue engineering. Mater Sci Technol. 2014;31(2):167–73.

38. Rau C, Wagner UH, Vila-Comamala J, Bodey A, Parson A, García-Fernández M, et al. Micro- and nano-imaging at the diamond beamline I13L-imaging and coherence. AIP Conf Proc. 2016;1741(July).

39 Pešić Z, De Fanis A, Wagner U and Rau C. Experimental stations at I13 beamline at Diamond Light Source. Journal of Physics: Conference Series. 2013;425:182003

40. Rau C, Wagner U, Pešić Z and De Fanis A. Coherent imaging at the Diamond beamline I13. physica status solidi (a). 2011;208:2522–2525.

41. Basham M, Filik J, Wharmby MT, Chang PC, El Kassaby B, Gerring M, Aishima J, Levik K, Pulford BC, Sikharulidze I, Sneddon D, Webber M,, Dhesi SS, Maccherozzi F, Svensson O, Brockhauser S, Náray G, Ashton AW. Data Analysis WorkbeNch (DAWN), Journal of synchrotron radiation. 2015;22(3):853-858

42. Ma PX. Biomimetic Materials for Tissue Engineering. Adv Drug Deliv Rev. 2008;60(2):184–98.

43. Bhattarai SR, Bhattarai N, Yi HK, Hwang PH, Cha D Il, Kim HY. Novel biodegradable electrospun membrane: Scaffold for tissue engineering. Biomaterials. 2004;25(13):2595–602.

44. Giuliani A, Erratico S, Torrente Y, Mazzoni S, Calcaterra F, Albertini G, et al. Polyglycolic Acid–Polylactic Acid Scaffold Response to Different Progenitor Cell In Vitro Cultures: A Demonstrative and Comparative X-Ray Synchrotron Radiation Phase-Contrast Microtomography Study. Tissue Eng Part C Methods. 2013;20(4):308-16.

45. Hyman AH and Simons K. Beyond HeLa cells. Nature comment. (2011) 480:34.

46 Giuliani et al. 2018. Phase-Contrast Microtomography: are the tracers necessary for Stem Cell Tracking in Infarcted Hearts? Biomedical Physics and Engineering Express 4: 055008,

47. Hollister SJ. Porous scaffold design for tissue engineering. Nat Mater. 2005;4:518–24.

48. Causa F, Netti PA, Ambrosio L. A multi-functional scaffold for tissue regeneration: The need to engineer a tissue analogue. Biomaterials. 2007;28(34):5093–9.

49. Shkarina S, Shkarin R, et al. 3D biodegradable scaffolds of polycaprolactone with silicate-containing hydroxyapatite microparticles for bone tissue engineering: high-resolution tomography and in vitro study. Scientific Reports 2018;8:8907.

50.. Gorodzha SN, Muslimov AR et al. A comparison study between electrospun polycaprolactone and piezoelectric poly(3-hydroxybutyrate-co-3-hydroxyvalerate) scaffolds for bone tissue engineering. 2017; Colloids Surf B Biointerfaces.160:48-59.

51. Ivanova AA, Syromotina DS et al. Effect of low-temperature plasma treatment of electrospun polycaprolactone fibrous scaffolds on calcium carbonate mineralisation, RSC ADVANCES. 2018; 8(68), 39106-39114

52. Urszula S, Szewczyk P, Kruk A, Barber A, Czyrska-Filemonowicz A. 3D imaging via FIB-SEM tomography at nanoscale for tissue engineering applications. Epicier T, editor. Proc. European Microscopy Congress. Lyon: Viley-VCH Verlag; 2016;318-319.

53.Carannante V, Önfelt B, Hertz HM, Fogelqvist E, Kördel M. Laboratory cryo x-ray microscopy for 3D cell imaging. Sci Rep. 2017;7(1):1–8.